Available online at www.sciencedirect.com
ScienceDirect
Journal of Photochemistry and Photobiology A: Chemistry 185 (2007) 331–337
Journal of Photochemistry and Photobiology A:Chemistry
www.elsevier.com/locate/jphotochem

A high molar extinction coefficient charge transfer sensitizer and its application in dye-sensitized solar cell

Md. K. Nazeeruddin [a,*], T. Bessho [b], Le Cevey [a], S. Ito [a], C. Klein [a], F. De Angelis [c], S. Fantacci [c], P. Comte [a], P. Liska [a], H. Imai [b], M. Graetzel [a]

[a] *Laboratory for Photonics and Interfaces, Institute of Chemical Sciences and Engineering, Ecole Polytechnique Fédérale de Lausanne, Station 6, CH-1015 Lausanne, Switzerland*
[b] *Environmental Material Laboratory, Material Science of Engineering, Graduate School of Engineering, Shibaura Institute of Technology, Shibaura, Minatoku, Tokyo, Japan*
[c] *Istituto CNR di Scienze e Tecnologie Molecolari (ISTM-CNR), c/o Dipartimento di Chimica, Università di Perugia, I-06123 Perugia, Italy*

Received 31 March 2006; received in revised form 27 June 2006; accepted 28 June 2006
Available online 7 August 2006

Abstract

A high molar extinction coefficient charge transfer sensitizer tetrabutylammonium [Ru(4,-carboxylic acid-4′-carboxylate-2,2′-bipyridine)(4,4′-di-(2-(3,6-dimethoxyphenyl)ethenyl)-2,2′-bipyridine)(NCS)$_2$], is developed which upon anchoring onto nanocrystalline TiO_2 films exhibit superior power conversion efficiency compared to the standard sensitizer bistetrabutylammonium *cis*-dithiocyanatobis(4,4′-dicarboxylic acid-2,2′-bipyridine)ruthenium(II) (N719). The new sensitizer anchored TiO_2 films harvest visible light very efficiently over a large spectral range and produce a short-circuit photocurrent density of 18.84 mA/cm^2, open-circuit voltage 783 mV and fill factor 0.73, resulting remarkable solar-to-electric energy conversion efficiency (η) 10.82, under Air Mass (AM) 1.5 sunlight. The Time Dependent Density Functional Theory (TDDFT) excited state calculations of the new sensitizer show that the first three HOMOs have ruthenium t_{2g} character with sizable contribution coming from the NCS ligands and the π-bonding orbitals of the 4,4′-di-(2-(3,6-dimethoxyphenyl)ethenyl)-2,2′-bipyridine. The LUMO is a π^* orbital localized on the 4,4′-dicarboxylic acid-2,2′-bipyridine ligand.

Keywords: High molar extinction coefficient charge transfer sensitizer; Nanocrystalline TiO_2 films; Dye-sensitized solar cells; Ruthenium sensitizer; Heteroleptic ruthenium complex

1. Introduction

Dye-sensitized solar cells (DSSC) based on mesoporous nanocrystalline TiO_2 films are potentially low cost and can reach light to electric power conversion efficiencies of 8–10% [1–3]. In these cells the sensitizer is one of the key components for high power conversion efficiency [4–7]. The pioneering studies on dye-sensitized nanocrystalline TiO_2 films using bis tetrabutylammonium *cis*-dithiocyanatobis-2,2′-bipyridine-4-COOH,4′-COO$^-$-ruthenium(II) (N719), is a paradigm in this field [8,9]. In spite of this, the main drawback of this sensitizer is the lack of absorption in the red region of the visible spectrum and also relatively low molar extinction coefficient. Therefore, our research is focused on at increasing the molar extinction coefficient of sensitizers, so that dye solar cells could be made thinner and thus more efficient because of reduced transport losses in the nanoporous environment. In quest of such sensitizers we have developed a high molar extinction coefficient sensitizer, tetrabutylammonium [Ru(4,-carboxylic acid-4′-carboxylate-2,2′-bipyridine)(4,4′-di-(2-(3,6-dimethoxyphenyl)ethenyl)-2,2′-bipyridine)(NCS)$_2$] (which here after labeled as N945), constituted of different ligands with specific functionality. The purpose of incorporating carboxylic acid groups in the 4,4′-position of 2,2-bipyridine ligand is two-fold: to graft the dye on the semiconductor surface, and to provide intimate electronic coupling between its excited state wave-function and the conduction band manifold of the semiconductor. The role of the thiocyanato ligands is to tune

* Corresponding author. Tel.: +41 21 6936124, fax: +41 21 6934111.
E-mail address: MdKhaja.Nazeeruddin@epfl.ch (Md.K. Nazeeruddin).

1010-6030/$ – see front matter © 2006 Elsevier B.V. All rights reserved.
doi:10.1016/j.jphotochem.2006.06.028

the metal t_{2g} orbitals of ruthenium(II) and possibly to stabilize the hole that is being generated on the metal, after having injected an electron into the conduction band. The function of 4,4′-di-(2-(3,6-dimethoxyphenyl)ethenyl)-2,2′-bipyridine ligand that contains extended π-conjugation with substituted methoxy groups to enhance molar extinction coefficient of the sensitizer; and furthermore, to tune the LUMO level of the ligand to provide directionality in the excited state. In this paper, we compare the photovoltaic properties, and Time Dependent Density Functional Theory (TDDFT) excited state calculations of this new sensitizer with the standard sensitizer bistetrabutylammonium *cis*-dithiocyanatobis(4,4′-dicarboxylic acid-2,2′-bipyridine)ruthenium(II).

2. Results and discussion

The 4,4′-di-(2-(3,6-dimethoxyphenyl)ethenyl)-2,2′-bipyridine ligand was conveniently synthesized by reaction of solid *tert*-BuOK with 4,4′-dimethyl-2,2′-bipyridine and 2,5-dimethoxybenzaldehyde in anhydrous DMF yielding 73% (see Section 3). The absorption spectra of 4,4′-di-(2-(3,6-dimethoxyphenyl)ethenyl)-2,2′-bipyridine in dichloromethane show bands in the UV region at 232 nm ($\varepsilon = 33{,}140$), 268 nm ($\varepsilon = 36{,}510$), 300 nm ($\varepsilon = 54{,}300$) and 358 nm ($\varepsilon = 40{,}410$) due to π–π^* charge transfer transitions [10,11]. Upon excitation at 350 nm, a dilute (5×10^{-7} M) solution of the ligand in dichloromethane at 298 K, exhibited intense emission centered at 450 nm with 43% quantum yields (Fig. 1), due to substitution of donor methoxy groups on the phenyl ring, in the *ortho*- and *meta*-positions. The position of the methoxy groups is vital for high quantum yields and the other isomers 4,4′-di-(2-(3,4-dimethoxyphenyl)ethenyl)-2,2′-bipyridine, 4,4′-di-(2-(2,4,6-trimethoxyphenyl)ethenyl)-2,2′-bipyridine show significantly low quantum yields in solution at room temperature.

The tetrabutylammonium [Ru(4,-carboxylic acid-4′-carboxylate-2,2′-bipyridine)(4,4′-di-(2-(3,6-dimethoxyphenyl)ethenyl)-2,2′-bipyridine)$(NCS)_2$] (N945), complex was synthesized

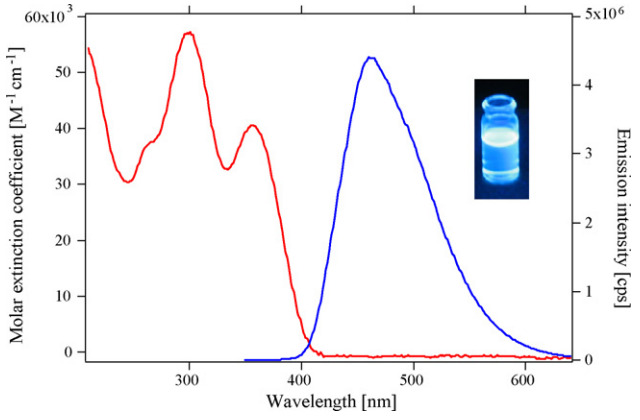

Fig. 1. Absorption (red line) and emission (blue line) spectra of the 4,4′-di-(2-(3,6-dimethoxyphenyl)ethenyl)-2,2′-bipyridine in dichloromethane solution λ_{ex} 350 nm, at 298 K. The inset shows a photo of the ligand solution exhibiting very strong blue emission, when excited under an ultraviolet lamp (365 nm).

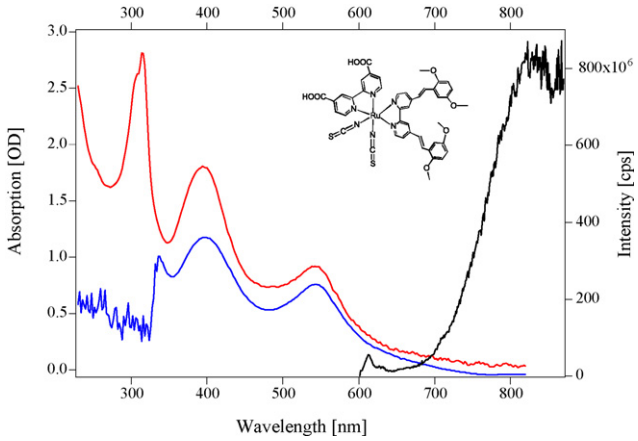

Fig. 2. UV/vis absorption spectra of N945 complex recorded as solution 5×10^{-5} M in 1:1 acetonitrile and *tert*-butanol (red line) and adsorbed on a nanocrystalline 2 μm thick transparent TiO_2 film (blue line, a similar 2 μm thick TiO_2 nanocrystalline film was used as reference. Below 335 nm is due glass absorption). The black line shows emission spectra of the same solution by λ_{ex} 550 nm, at 298 K. The inset shows chemical structure of the N945 complex.

using our previously reported procedure [11]. The absorption spectrum of the N945 sensitizer is dominated by metal to ligand charge transfer transitions (MLCT) in the visible region with the lowest allowed MLCT bands appearing at 400 and 550 nm. The molar extinction coefficients of these bands are 34,500 and 18,900 M^{-1} cm^{-1}, respectively (Fig. 2), which are significantly higher (≈40%) when compared to than that of the standard sensitizer *cis*-dithiocyanatobis(4,4′-dicarboxylic acid-2,2′-bipyridine)ruthenium(II) (N3) [8]. The absorption spectra of both N945 adsorbed on a 2 μm TiO_2 film show features similar to those seen in the corresponding solution spectra (see Fig. 2). When the N945 sensitizer is excited within the MLCT absorption band at 298 K in an air-equilibrated 1:1 acetonitrile and *tert*-butanol solution, it exhibits a luminescence maximum at 825 nm (Fig. 2) with an excited state lifetime of 27 ns in degassed solution.

The N945 sensitizer anchored onto a double layered nanocrystalline TiO_2 film (see Section 3) and measured its photovoltaic properties (Fig. 3) using with an electrolyte consisting of 0.60 M 1-butyl-3-methylimidazolium iodide (BMII), 0.03 M I_2, 0.10 M guanidinium thiocyanate and 0.50 M *tert*-butylpyridine in a mixture of acetonitrile and valeronitrile (volume ratio: 85:15). The incident monochromatic photon-to-current conversion efficiency (IPCE) plotted as a function of excitation wavelength shows 91% in the visible region. From the overlap integral of this curve one measures a short-circuit photocurrent density of 18.76 mA/cm^2. In agreement with this measurement the N945-sensitized cell gave under standard global Air Mass (AM) 1.5 solar condition, a short-circuit photocurrent density (i_{sc}) of 18.84 ± 0.2 mA/cm^2, the open-circuit voltage was 785 ± 30 mV and a fill factor of 0.73 ± 0.03, corresponding to an overall conversion efficiency η, derived from the equation: $\eta = i_{sc} V_{oc}$ ff/light intensity of 10.80%.

Dye-sensitized solar cells with electrolyte containing low-boiling point solvents are not practicable for long-term applica-

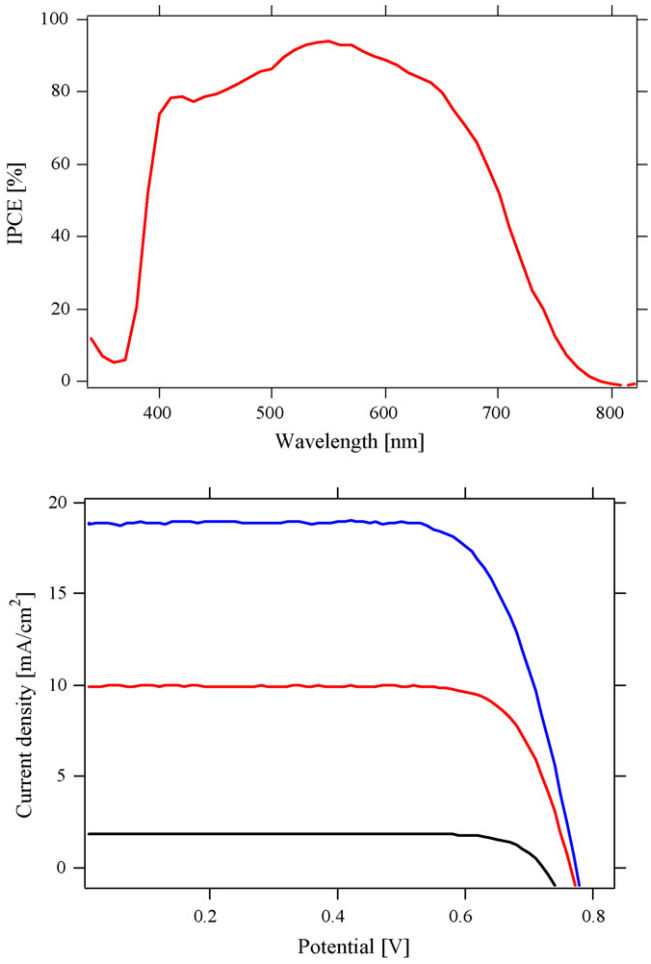

Fig. 3. Incident photon-to-current conversion efficiency plotted as a function of excitation wavelength (top), and photocurrent–voltage characteristics of a solar cell based on 12 + 3 μm TiO_2 film sensitized by N945 (bottom). The photocurrent–voltage data measured using 0.156 cm^2 cell using a mask under illumination of 99 mW/cm^2 blue curve; 51 mW/cm^2 red curve; 10 mW/cm^2 black curve.

tions. Therefore, we have used thermally stable electrolyte composed of 0.8 M 1,2-dimethyl-3-propylimidazolium iodide, 0.1 M I_2 and 0.5 M *N*-methylbenzimidazole in 3-methoxypropionitrile (Robust), which is a low vapour pressure and high boiling solvent [12]. Using this electrolyte system, the photovoltaic performance of the N945 sensitizer strikingly, exhibited a short-circuit photocurrent density of density of 17.79 ± 0.5 mA/cm^2, 728 ± 20 mV open-circuit potential and 0.71 ± 0.05 fill factor, yielding a power conversion efficiency of 9.2% at AM 1.5 sunlight. Under similar conditions our best sensitizer [Ru(4,-carboxylic acid-4′-carboxylate-2,2′-bipyridine)(4,4′-di-(2-(4-hexyloxyphenyl)ethenyl)-2,2′-bipyridine)$(NCS)_2$] (K19), which contains only one alkoxy group at *para*-position gave a short-circuit photocurrent density of 15.1 mA/cm^2, an open-circuit photovoltage of 747 mV and 0.69 fill factor, yielding an overall conversion efficiency (η) of 8.0% [12,13]. Table 1 illustrates the photovoltaic performance characteristics of the N945, N719 and K19 sensitizers at different incident light intensities. The N945-sensitized solar cell at half sun gave short-circuit photocurrent density of 9.7 ± 0.5 mA/cm^2, 710 ± 20 mV open-circuit potential and 0.74 ± 0.05 fill factor, resulting a power conversion efficiency of 9.91%. The increased efficiency of both the N945 and the K19 sensitizers at half sun compared to the one sun is mainly due to the improved fill factor.

From the electronic and photovoltaic data it is apparent that the significant effect asserted by the N945 sensitizer that contains 4,4′-di-(2-(3,6-dimethoxyphenyl)ethenyl)-2,2′-bipyridine ligand with donor groups in the *ortho*- and *meta*-positions compared to the K19 sensitizer [13].

In order to see the impact of high molar extinction coefficients of the N945 sensitizer on photovoltaic properties compared to the standard N719 sensitizer, we have fabricated solar cells using both the sensitizers with transparent TiO_2 membrane of various thicknesses. The performance characteristics of both the N945 and N719 sensitizers were obtained with the electrolyte containing 0.60 M butylmethylimidazolium iodide (BMII), 0.03 M I_2, 0.10 M guanidinium thiocyanate and 0.50 M *tert*-butylpyridine in a mixture of acetonitrile and valeronitrile (volume ratio: 85:15). Fig. 4a displays incident photon-to-current conversion efficiency plotted as a function of excitation wavelength of the N945 and N719 sensitizers with 2 μm transparent TiO_2 membranes. The IPCE spectra exhibit a maximum of 61% for the N945 sensitizer, which is only 50% for N719 sensitizer. From the overlap integral of these curves, one predicts a short-circuit photocurrent density of 9.0 and 7.0 mA/cm^2, respectively. At standard global AM 1.5 solar conditions, the N945 cell gave a photocurrent density of (I_{sc}) 9.3 mA/cm^2, open-circuit potentials of (V_{oc}) 809 mV and a fill factor (ff) of 0.76, yielding 5.72% conversion efficiency. Under similar conditions, the N719-sensitized solar cell showed 7.27 mA/cm^2 I_{sc}, 819 mV V_{oc} and 0.76 ff, yielding a conversion efficiency of 4.56%. The higher efficiency

Table 1
Photovoltaic parameters of DSSC under different light intensities using the Robust electrolyte with N945, K19 and N719 sensitizers

Sensitizer	Light intensity (mW/cm^2)	J_{sc} (mA/cm^2)	V_{oc} (mV)	Fill factor	Efficiency, η (%)
N945	51.3	9.71	710	0.748	9.91
	100	17.96	728	0.71	9.29
K19	51.3	8.2	728	0.734	8.5
	100	15.1	747	0.699	8.0
N719	51.3	8.52	765	0.77	9.48
	100	15.82	785	0.75	9.31

The data of K19 were taken from references [12,13].

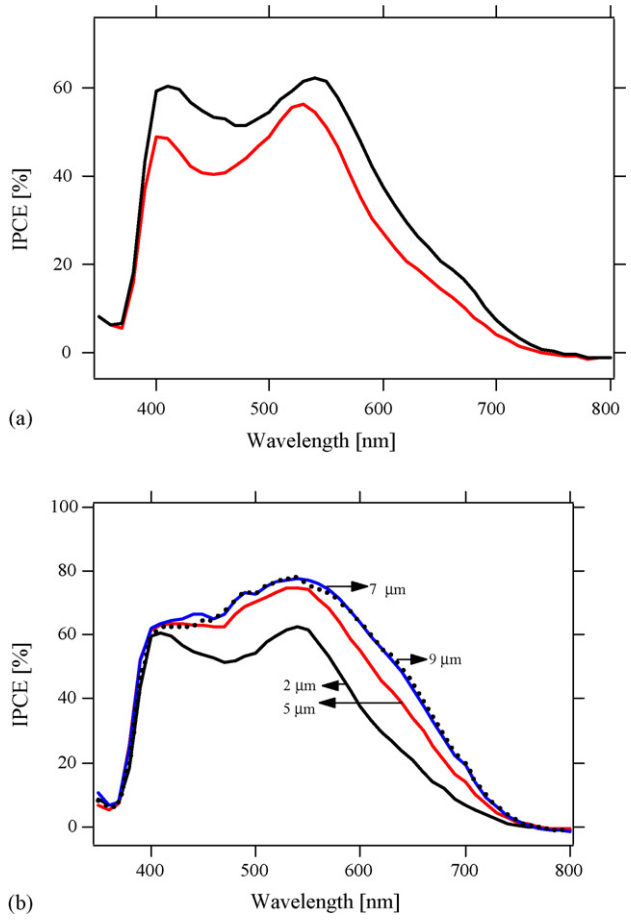

Fig. 4. (a) Comparison of incident photon-to-current conversion efficiencies plotted as a function of excitation wavelength for N945 (black line) and the N719 (red line) sensitizers, which were anchored onto a 2 μm transparent TiO_2 membranes. (b) Comparison of incident photon-to-current conversion efficiencies plotted as a function of excitation wavelength for N945 with different membrane thicknesses, 2 μm (black line); 5 μm (red line); 7 μm (blue line); 9 μm (black dotted line).

of the N945 dye-sensitized solar cell is caused by stronger light absorbance of N945 across the visible spectrum with superior response in the red region.

Fig. 4b and Table 2 illustrate the comparison of IPCE and photovoltaic data, respectively obtained using N945 and N719 sensitizers with transparent TiO_2 membrane of various thicknesses. The data show that as the membrane thickness decreased, less photocurrent is produced due to the incident light is not fully absorbed by the adsorbed dye. The J_{sc} increases continuously with film thickness reaching a plateau value of close to 19 mA/cm^2 at 14 μm while efficiency (η) reaches a maximum of 10.82%. On the contrary, the open-circuit potential decreased with increasing membrane thickness [14]. The data demonstrate that the N945 photovoltaic performance is superior compared to the N719 sensitizer for thinner membranes. The I_{sc} of N945 is ≈30% higher compared to the I_{sc} of N719 on a 2 μm TiO_2 thick membrane consistent with the high molar extinction coefficient of the N945 dye. However, for thicker TiO_2 membranes of 9 μm the disparity in efficiency between the two sensitizers decreases from 30 to less than 7%. For thicker TiO_2 membrane of 9 μm and above, and scattering double layers of 12 + 3 μm, an upper bound limit is reached beyond which the influence of dye high molar extinction coefficient is buffered (see Fig. 4b).

Table 3
Stability data of N945 sensitizer adsorbed on 7 + 3 μm thick TiO_2 membrane and the Robust electrolyte at 80 °C

Time in days	J_{sc} (mA/cm^2)	V_{oc} (mV)	Fill factor	Efficiency, η (%)
1	15.1	692	0.73	7.59
4	15.6	700	0.71	7.73
11	15.3	668	0.71	7.31
17	16.2	671	0.70	7.60
30	16.1	643	0.70	7.19
36	16.0	633	0.70	7.0

The N945 dye-sensitized solar cells were subjected to accelerated testing in a solar simulator at 100 mW/cm^2 intensity and thermal aging in an oven at 80 °C. Table 3 shows short-circuit current, open-circuit potential, fill factor and the efficiency data of obtained over 36 days using double layer of 7 + 3 μm thick TiO_2 membrane and the Robust electrolyte. During the aging process the short-circuit current increased from 15.1 to 16 mA/cm^2 however, the open-circuit potential decreased from 692 to 633 mV. The data show that the overall efficiency remained 93% of the initial value after 36 days of thermal stress at 80 °C.

Table 2
Comparison of photovoltaic parameters of N945 and N719 sensitizers with different transparent TiO_2 membrane thickness using an electrolyte of having composition of 0.60 M butylmethylimidazolium iodide (BMII), 0.03 M I_2, 0.10 M guanidinium thiocyanate and 0.50 M *tert*-butylpyridine in a mixture of acetonitrile and valeronitrile (volume ratio: 85:15) under 99 mW/cm^2 light intensity

TiO_2 film thickness (μm)	Sensitizers	IPCE (%)	J_{sc} (mA/cm^2)	V_{oc} (mV)	Fill factor	Efficiency, η (%)
2	N945	61	9.30	809	0.76	5.72
	N719	50	7.27	819	0.76	4.56
5	N945	74	12.12	783	0.76	7.31
	N719	67	9.94	810	0.77	6.19
7	N945	77	13.42	782	0.75	8.04
	N719	76	11.73	797	0.77	7.21
9	N945	76	13.94	772	0.77	8.31
	N719	79	12.86	788	0.76	7.78

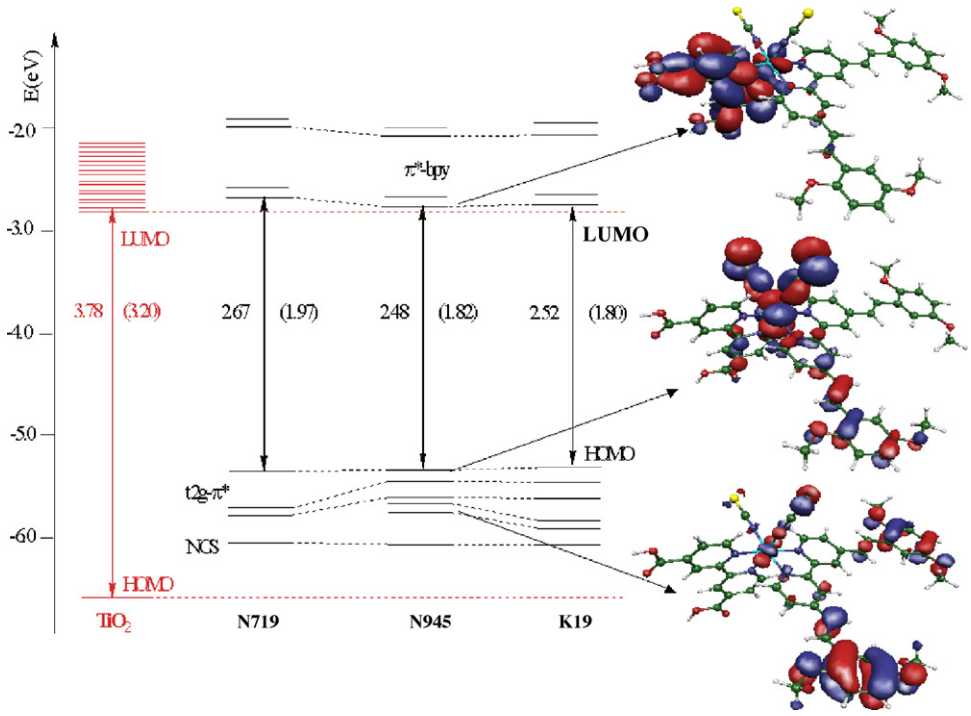

Fig. 5. Molecular orbital energy diagram of N719, N945 and K19 compared to that of a TiO_2 nanoparticle model. HOMO–LUMO gaps (eV) and lowest TDDFT excitation energies (eV, data in parenthesis) are reported together with isodensity plots of the HOMO-3, HOMO and LUMO of the N945 complex.

2.1. Computational study

To gain insight into the electronic structure of the N945 and K19 dyes we performed DFT geometry optimizations and Time Dependent DFT excited state calculations at the B3LYP/3-21G* [15,16] level in water solution, by means of the C-PCM solvation model [17,18] implemented in the Gaussian03 package [19]. The results are compared in Fig. 5 with the corresponding data for the N719 dye and for a model TiO_2 nanoparticle [9,20]. For both N719, N945 and K19 the first three HOMOs have ruthenium t_{2g} character with sizable contribution coming from the NCS ligands; for N945 and K19 extensive mixing of these Ru-NCS combinations with π-bonding orbitals of the 4,4′-di-(2-(3,6-dimethoxyphenyl)ethenyl)-2,2′-bipyridine and 4,4′-di-(2-(4-hexyloxyphenyl)ethenyl)-2,2′-bipyridine, respectively, takes place (see Fig. 5). For N719 the HOMO-3 is a non-bonding combination localized on the NCS ligands, while in N945 and K19 two π-bonding orbitals of the 4,4′-di-(2-(3,6-dimethoxyphenyl)ethenyl)-2,2′-bipyridine and 4,4′-di-(2-(4-hexyloxyphenyl)ethenyl)-2,2′-bipyridine, respectively, ligand insert among the Ru-NCS orbitals (see Fig. 5). This mixing of Ru-NCS and bipyridine ligand π orbitals might be responsible of the increased absorbance of N945 and K19 with respect to N719.

For N945 and K19 the LUMO is a π^* orbital localized on the 4,4′-dicarboxylic acid-2,2′-bipyridine ligand (see Fig. 5), while the LUMO + 1 is a π^* combination localized on the 4,4′-di-(2-(3,6-dimethoxyphenyl)ethenyl)-2,2′-bipyridine and 4,4′-di-(2-(4-hexyloxyphenyl)ethenyl)-2,2′-bipyridine, respectively, ligand. For N719, on the other hand, the LUMO/LUMO + 1 are delocalized over the two bipyridine ligands, with maximum components on the pyridines bearing the protonated carboxylic groups. As it can be noted from Fig. 5, the LUMO and LUMO + 1 of N945 and K19 are slightly stabilized and show a favorable alignment with the TiO_2 conduction band edge, which is consistent with the high photocurrents measured experimentally. The N945 and K19 LUMO + 2/LUMO + 3 complexes have a similar character has the LUMO/LUMO + 1 couple.

The electronic structure of the N945 and K19 sensitizers is quite similar: the energy and localization of the unoccupied orbitals is essentially the same in the two complex while the most noticeable difference is a stabilization of π-bonding orbitals of the 4,4′-di-(2-(4-hexyloxyphenyl)ethenyl)-2,2′-bipyridine in K19, which are calculated to lie ca. 0.2 eV below the corresponding 4,4′-di-(2-(3,6-dimethoxyphenyl)ethenyl)-2,2′-bipyridine π-bonding orbitals in N945. The similar electronic structure translates into a similar lowest excitation energy for the two species, which essentially corresponds to a HOMO–LUMO transition.

2.2. Conclusions and perspectives

We have demonstrated functionalization of ruthenium complex resulting in enhanced molar extinction coefficient, and creating directionality in the excited state of the sensitizer by adjusting the electron densities of donor moieties that are not attached to the TiO_2 surface. Thus, this class of compounds serves as the basis for the design of novel compounds containing further extended π-system with different donor groups, which are expected to increase significantly molar extinction coefficient and show panchromatic response. We are currently examining related complexes that contain substituents in

both the *ortho*-, *meta*- and *para*-positions of the π-extended ligand.

3. Experimental

3.1. Materials and measurements

All the solvents and chemicals unless stated otherwise, were purchased from Fluka, puriss grade. UV/vis and fluorescence spectra were recorded in 1 cm path length quartz cell on a Cary 5 spectrophotometer and Spex Fluorolog 112 Spectrofluorimeter, respectively. Proton and ^{13}C NMR spectra were measured on a Bruker 200 MHz spectrometer. The reported chemical shifts were in ppm against TMS.

3.2. Synthesis of 4,4′-di-(2-(2,5-dimethoxyphenyl)ethenyl)-2,2′-bipyridine (N945L)

The 4,4′-di-(2-(3,6-dimethoxyphenyl)ethenyl)-2,2′-bipyridine was conveniently synthesized by reaction of solid *tert*-BuOK with 4,4′-dimethyl-2,2′-bipyridine and 2,5-dimethoxybenzaldehyde in anhydrous DMF yielding 73% [21]. In a typical one-pot synthesis solid *t*BuOK (7.31 g, 65.1 mmol) was added in one portion to a mixture of 4,4′-dimethyl-2,2′-bipyridine (3.00 g, 16.3 mmol) and 2,5-dimethoxybenzaldehyde (8.12 g, 48.8 mmol) in anhydrous DMF (200 ml). The resulting mixture was heated to 100 °C for 6 h under nitrogen. After being cooled to room temperature, DMF was evaporated and methanol (200 ml) was added resulting in the formation of a yellow precipitate. The solid was filtered and washed with methanol (5 × 50 ml) to afford 5.7 g (73%) of the desired compound as a blue fluorescent solid. The DSC curve of N945L shows a sharp melting temperature of 195 °C.

^1H NMR ($CDCl_3$) δ 8.69 (2H, d, $J = 4.8$ Hz, pyridine), 8.61 (2H, s, pyridine), 7.47 (2H, $J = 16.4$ Hz, d, vinylic), 7.43 (2H, d, $J = 4.8$ Hz, pyridine), 7.32 (2H, t, $J = 7.6$ Hz, methoxyphenyl), 7.18 (2H, d, methoxyphenyl), 7.14 (4H, d, $J_1 = 16$ Hz, broad s, vinylic + methoxyphenyl), 6.90 (1H + 1H, d, $J_1 = 7.6$ Hz, broad s), 3.87 (s, 12H, –OCH_3). ^{13}C NMR, 49.5, 148.9, 133.3, 129.8, 126.4, 124.9, 122.2, 121.1, 119.7, 118.4, 114.5, 112.1, 55.3, 21.2. IR (KBr) 3306, 2937, 1598, 1487, 1462, 1435, 1263, 1149, 1046, 783, 700. Anal. Calcd. for $C_{30}H_{28}N_2O_4$: C, 74.98; H, 5.87; N, 5.83; Found: C, 74.69; H, 6.11; N, 5.84.

The heteroleptic complex [Ru(4,-carboxylic acid-4′-carboxylate-2,2′-bipyridine)(4,4′-di-(2-(3,6-dimethoxyphenyl)ethenyl)-2,2′-bipyridine)$(NCS)_2$] (N945) was synthesized using our previously reported one-pot procedure and characterized with electrochemical and spectroscopic techniques [22].

The working and the counter electrodes for dye-sensitized solar cells were prepared using the following procedure. The FTO glass plates (Solar 4 mm thickness, Nippon Sheet Glass) were first cleaned in a cleaning detergent aqueous solution with an ultrasonic bath for 15 min, washed out with water and ethanol. After treated by UV-O_3 cleaning system (Model No. 256-220, Jelight Company, Inc.) for 18 min, the electrodes were immersed into 40 mM $TiCl_4$ *aq.* at 70 °C for 30 min and washed out with water and ethanol. Two kinds of TiO_2 paste containing nanocrystalline (20 nm) TiO_2 (paste A) and submicroparticle (400 nm) TiO_2 (paste B) were prepared by a procedure previously reported [23]. The screen printing procedure with the paste A (coating, keeping and drying) was repeated to get appropriate thickness of TiO_2 films (2–14 μm). After drying paste A at 125 °C, paste B was further coated two times, resulting that the thickness of TiO_2 films with 400 nm particles for the light scattering layer was 3–4 μm. The electrodes coated with TiO_2 pastes were gradually heated under air flow at 325 °C for 5 min, at 375 °C for 5 min, at 450 °C for 15 min and 500 °C for 15 min. Then the electrodes were treated with 40 mM $TiCl_4$. After the treatment the TiO_2 films was rinsed with water and ethanol and sintered again at 500 °C for 30 min. At 80 °C in the cooling time, the TiO_2 electrodes were immersed into dye solutions (0.3 mM in a mixture of acetonitrile and *tert*-butyl alcohol (volume ratio: 1:1)) and kept at room temperature for 20–24 h.

For the counter electrode, a FTO plate (TEC 15/2.2 mm thickness, Libbey-Owens-Ford Industries) was drilled by sand blaster and cleaned with ultrasonic bath in H_2O, acetone and 0.1 M HCl *aq*., subsequently. The counter electrodes were prepared by coating a drop of H_2PtCl_6 solution (2 mg Pt in 1 ml ethanol) on the FTO and heating at 400 °C for 15 min.

The dye-adsorbed TiO_2 electrode and Pt-counter electrode were assembled into a sandwich sealed type cell by heating with a hot-melt ionomer film (Surlyn 1702, 25 μm thickness, Du-Pont) as a spacer between the electrodes. A drop of electrolyte solution (0.60 M 1-butyl-3-methylimidazolium iodide (BMII), 0.03 M I_2, 0.10 M guanidinium thiocyanate and 0.50 M *tert*-buthylpyridine in a mixture of atetonitryl and varironitryl, volume ratio: 85:15) was put on the hole drilled in the counter electrode of assembled cell. Subsequently, the cell was put in a small chamber and the air of the chamber and the inside of the cell was pumped out until finishing the bubbling of the electrolyte for 5–10 s. The stop of the vacuum and the ventilation of the ambient air injected the electrolyte into the cell. Finally, the hole was sealed using a hot-melt ionomer film (Bynel 4702, 35 μm thickness, Du-Pont) and a cover glass (0.1 mm thickness) by heating.

Acknowledgements

We acknowledge financial support of this work by the Swiss Science Foundation and Swiss Federal Office for Energy (OFEN). We thank Dr. S.M. Zakeeruddin, Dr. Peter Péchy for providing electrolytes and Dr. Robin Humphry-Baker for his kind assistance.

References

[1] K.D. Benkstein, N. Kopidakis, J. van de Lagemaat, A.J. Frank, J. Phys. Chem. B 107 (2003) 7759.
[2] W. Kubo, T. Kitamura, K. Hanabusa, Y. Wada, S. Yanagida, Chem. Commun. (2002) 374.
[3] Z.-S. Wang, Y. Yamaguchi, H. Sugihara, H. Arakawa, Langmuir 21 (2005) 4272.
[4] M.K. Nazeeruddin, P. Péchy, T. Renouard, S.M. Zakeeruddin, R. Humphry-Baker, P. Comte, P. Liska, C. Le, E. Costa, V. Shklover, L. Spiccia, G.B.

Deacon, C.A. Bignozzi, M. Grätzel, J. Am. Chem. Soc. 123 (2001) 1613.
[5] Y. Takahashi, H. Arakawa, H. Sugihara, K. Hara, A. Islam, R. Katoh, Y. Tachibana, M. Yanagida, Inorg. Chim. Acta 310 (2000) 169.
[6] S. Altobello, R. Argazzi, S. Caramori, C. Contado, S. Da Fré, P. Rubino, C. Choné, G. Larramona, C.A. Bignozzi, J. Am. Chem. Soc. 127 (2005) 15342.
[7] G. Sauvé, M.E. Cass, S.J. Doig, I. Lauermann, K. Pomykal, N.S. Lewis, J. Phys. Chem. 104 (2000) 3488.
[8] M.K. Nazeeruddin, A. Kay, I. Rodicio, R. Humphry-Baker, E. Muller, P. Liska, N. Vlachopoulos, M. Grätzel, J. Am. Chem. Soc. 115 (1993) 6382.
[9] M.K. Nazeeruddin, F. De Angelis, S. Fantacci, A. Selloni, G. Viscardi, P. Liska, S. Ito, T. Bessho, M. Grätzel, J. Am. Chem. Soc. 127 (2005) 16835.
[10] K.A. Walters, L.L. Premvardhn, Y. Liu, L.A. Peteanu, K.S. Schanze, Chem. Phys. Lett. 339 (2001) 255.
[11] M.K. Nazeeruddin, Q. Wang, L. Cevey, V. Aranyos, P. Liska, E. Figgemeier, C. Klein, N. Hirata, S. Koops, S.A. Haque, J.R. Durrant, A. Hagfeldt, A.B.P. Lever, M. Grätzel, Inorg. Chem. 45 (2006) 787.
[12] P. Wang, C. Klein, R. Humphry-Baker, S.M. Zakeeruddin, M. Grätzel, Appl. Phys. Lett. 86 (2005) 123508.
[13] P. Wang, C. Klein, R. Humphry-Baker, S.M. Zakeeruddin, M. Grätzel, J. Am. Chem. Soc. 127 (2004) 808.
[14] J.-J. Lee, G.M. Coia, N.S. Lewis, J. Phys. Chem. B 108 (2004) 5282.
[15] A.D.J. Becke, Chem. Phys. 98 (1993) 5648.
[16] J.S. Binkley, J.A. Pople, W.J. Hehre, J. Am. Chem. Soc. 102 (1980) 939.
[17] M. Cossi, V.J. Barone, J. Chem. Phys. 115 (2001) 4708.
[18] M. Cossi, N. Rega, G. Scalmani, V.J. Barone, J. Comp. Chem. 24 (2003) 669.
[19] M.J. Frisch et al., Pittsburgh, PA, 2003 (Supporting information available for complete reference).
[20] F. De Angelis, A. Tilocca, A. Selloni, J. Am. Chem. Soc. 126 (2004) 15024.
[21] V. Aranyos, J. Hjelm, A. Hagfeldt, H. Grennberg, Dalton Trans. (2003) 1280.
[22] S.M. Zakeeruddin, M.K. Nazeeruddin, R. Humphry-Baker, P. Péchy, P. Quagliotto, C. Barolo, G. Viscardi, M. Graetzel, Langmuir 18 (2002) 952.
[23] P. Wang, S.M. Zakeeruddin, P. Comte, R. Charvet, R. Humphry-Baker, M. Graetzel, J. Phys. Chem. B 107 (2003) 14336.